

In situ transmission electron microscopy mechanical deformation and fracture of a silver nanowire

Diego Alducin¹, Raul Borja¹, Eduardo Ortega¹, J. Jesus Velazquez-Salazar¹, Mario Covarrubias², Fernando Mendoza Santoyo^{1}, Lourdes Bazán-Díaz¹, John Eder Sanchez¹, Nayely Torres¹, Arturo Ponce¹ and Miguel José-Yacamán¹*

¹Department of Physics and Astronomy, University of Texas at San Antonio, San Antonio, Texas 78249, United States

²Department of Mechanical Engineering, Politecnico Di Milano, Campus Bovisa Sud – via La Masa 1, 20156 Milano, Italy

Abstract

In this paper a fivefold twinning silver nanowire is mechanically tested in real time within a transmission electron microscope using an atomic force microscopy sensor. Our experimental setup allows to measure, by bending the silver nanowire, the elastic modulus (E), the fracture toughness (K_{IC}) and the stress intensity factor (σ_I) for elastic and plastic deformation regions and finally the fracture of the nanowire. Data of the force applied and the bending of the nanowire was recorded during the deformation and after the point of fracture. Mechanical properties the nanowire were extracted and compared with nanoindentation using atomic force microscopy.

Keywords: Silver nanowires, in situ TEM measurements, mechanical deformation, transmission electron microscopy

*On sabbatical leave Centro de Investigaciones en Óptica, A.C. Loma del Bosque 115, León, Gto., 37150, México.

1. Introduction

In situ transmission electron microscopy (TEM) has opened the possibility to measure physical properties individually in nanostructures. Mechanical properties measured at nanoscale reveal modified regimes compared with their macroscale counterparts, such is the case of metallic nanoparticles and atomic-layers of transition metal dichalcogenides[1-2]. In addition, at nanoscale gravity forces is not appreciable and the surrounding forces of metallic nanoparticles can be measured with an experimental setup in which an atomic force microscopy (AFM) tip is coupled in a TEM sample holder [3]. Other metallic nanowires are also subject to be studied within a TEM to measure other physical properties such as magnetic behavior and their in situ magnetization by exciting the objective lens [4]. In this way, Silver (Ag) nanowires (NWs) have a special interest for measuring physical properties at individual motifs due to their optical properties. For instance Ag-NWs show interesting physical properties [5-7] and are good candidates for a large variety of applications such as plasmonic devices[8-9], plasmonic waveguides[10-11] and biosensors[12-13]. Different methods of synthesis have been reported a good control of their aspect ratio and how it can change their physical properties [14-16]. Novel techniques on the testing of the mechanical properties of nanostructures have been developed in recent years to perform resonance[17-19], bending[20-23] and tensile[24-25] tests. Previous research on the mechanical properties of the nanowires has not reported the live feedback of the behavior of the material during fracture after plastic deformation. Chen *et al.* [26] performed nanomechanical bending behavior and theoretical calculation of the elastic modulus of the silver nanowires using atomic force microscopy (AFM). However, there is few experimental research done on the failure and fracture of nanowires, for instance Wu *et al.* [27] performed three point bending on Ag NWs to observe the plastic deformation of hardened silver nanowires

in an atomic force microscope. In this work we report the elastic and plastic deformation until failure of an Ag-NW through an AFM holder coupled within a transmission electron microscope to perform a mechanical three point bending test. Video of the test was recorded where the mechanical deformation of NW begins and ends with total fracture. Detailed information of the force exerted by the tip until failure, the stress intensity factor, and the fracture toughness of the Ag NWs was measured from the recorded data. Additionally, the mechanical properties measured in TEM were compared via nanoindentation performed in an atomic force microscope.

2. Experimental Methods

Silver nitrate (AgNO_3), poly (Vinyl Pyrrolidone) (PVP, $M_w = 55\ 000$) and Ethylene Glycol (EG) were supplied by Sigma-Aldrich and used without further purification. Silver nanowires were synthesized by using polyol [28]. The synthesis methodology has been performed as follows: 5 ml of ethylene glycol was preheated at 160°C for 1 h under magnetic stirring in a rounded bottom flask, then 3 mL of AgNO_3 (0.1 M, in EG) and 3 mL of PVP (0.15 M, in EG) were simultaneously dropped into the hot solution (~ 0.2 mL/min). The reaction was let to boil for an additional 30 min. The solution changed from yellow to greenish gray indicating the formation of the Ag NWs. Subsequently the product is cooled at room temperature and washed with ethanol three times and two times with acetone followed by centrifugation at 1500 rpm during 15 min. Finally, the precipitate is dispersed in ethanol and a glossy gray solution is observed.

These nanowires characterized by their pentagonal cross section and large aspect ratio are shown in Figure 1. The changes in the coloration of the colloidal solution serves as a control during the growth of nanowires. In Figure 1(a) are presented images of the solution at different reaction stages, in which the yellow color of the solution is due to the formation of small particles (seeds).

After several minutes, the orange color indicates the formation of larger particles and the anisotropic growth takes place. Finally, the nanowire solution turns gray. Figure 1 (b) shows a magnified SEM image with the inset presenting a geometrical model of the transversal and longitudinal sections of a nanowire. The (100) and (111) facets are shown. These nanowires present a narrow diameter distribution as is noticed. The average diameter of the nanowires was ~60 nm and the length varied from 10 to 20 micrometers. The Ag nanowires were studied by high resolution transmission electron microscopy (HRTEM) using a JEOL 2010F microscope operated at 200 kV. In Figure 1 (c) the end of an individual Ag NW is presented. The Fast Fourier Transform (FFT) is also displayed in which the growth direction is easily noticed. The darker contrast in the image indicates the twinned nature of this wire. The nanowire growth is along $\langle 110 \rangle$ direction. From the high magnification micrograph shown in Figure 1(d), the measured lattice distances are 0.23 nm corresponding to the $\{111\}$ plane of the cubic structure of silver.

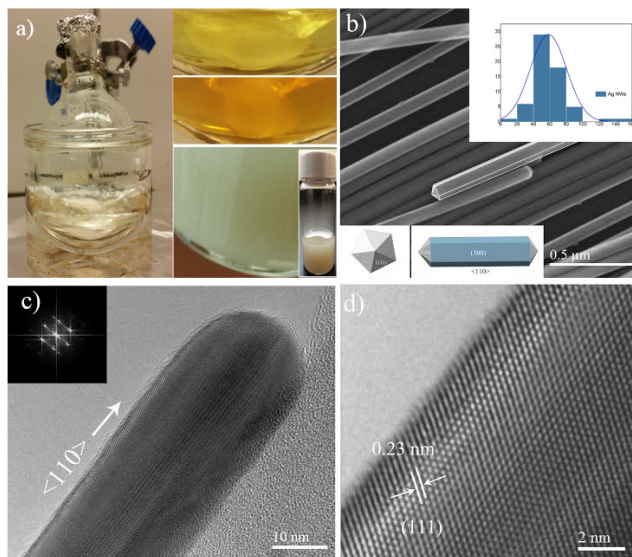


Figure 1. Micrographs of the synthesized Ag NWs. (a) Coloration changes during the synthesis process. (b) Low Magnification SEM image of the Ag NWs with a diameter histogram and simulations of the pentagonal cross sections as insets. (c) TEM micrograph of the tip of one

nanowire. The FFT shows the characteristic reflections of a twinned structure. (d) HRTEM image showing the interplanar spacing of the nanowire.

The in situ experiment was performed within a transmission electron microscope JEOL ARM200F operated at 200kV, using an in situ AFM holder (Nanofactory Instruments). This holder has a silicon tip and a reference cantilever to measure the applied load. With this instrument it is possible to observe the AFM tip in contact with the nanowire as it applies a load and creates the fracture as the load is increased. The AFM-TEM holder has a sapphire ball mounted on a piezotube that allows positioning and manipulation in (X, Y, Z) by coarse and fine movements (~1 nm) respectively[1, 29-30]. A single Ag NW was supported on the two ends on a gold surface in the three point bending configuration, see Figure 2. In Figure 2(a) we can observe the moment in which the AFM sensor creates contact with the NW in a three point bend test set up. Figure 2(b) is a model of the fivefold nanowire in the same set up.

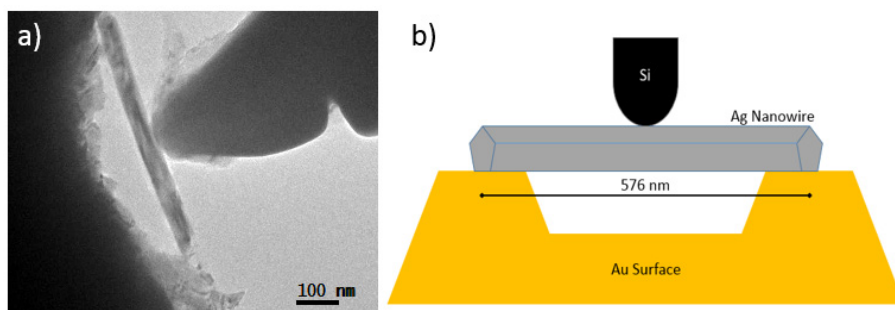


Figure 2 – a) TEM micrographs of the Ag NW. b) Three point bending configuration of the Ag NW with a length of 576nm. The surface contact of the AFM tip to the Ag NW has a length of 60nm.

In order to set the sample of Ag NWs in the AFM-TEM holder, a concentrated solution of pentagonal silver NWs was prepared and suspended in ethanol under constant stirring at room temperature, until the solution color turned beige to assure presence of NWs. A small volume (2

μl) of nanowire suspension was drop-casted onto a substrate (a flattened $250\ \mu\text{m}$ gold bondwire) which was then attached on a gold hat on top of the sapphire ball on the AFM-TEM holder. The diameter of the NW of $50\ \text{nm}$. The mechanical test of the Ag NW was recorded on video available in the supplementary material. The NW rested on the gold bondwire, and was finely approached towards the AFM tip at a $0.5\ \text{nm}$ steps by means of the piezotube. From the video it was possible to analyze the mechanical response of the Ag NW, in both elastic and plastic regimes, to an applied load. Estimation of variables such as the nanowire length between supported ends, deflection angle and displacement of the AFM tip, needed to estimate the Young's Modulus. In addition to the in situ experiment, AFM indentation experiments were performed using a Multimode NanoScope V. All measurements were taken in air at room temperature using a non-conductive silicon nitride (Si_3N_4) triangular cantilever triangular cantilevers (MLCT-F, Veeco Co.) with a length of $85\ \mu\text{m}$ and nominal spring constant of $0.6\ \text{N/m}$. The normal force was calibrated by recording the deflection of the cantilever as a function of the scanner displacement while in contact with a sapphire substrate. The normal force was calibrated by recording the deflection of the cantilever as a function of the scanner displacement while in contact with a silicon substrate. Data analysis was conducted using the NanoScope software on height images.

3. Results and discussion

As measured from the recorded video, individual images were extracted frame by frame as TEM images, the beam length between supported ends (L) was $475\ \text{nm}$. The average diameter (D) measured in the NW was $50\ \text{nm}$. The load of the tip on the NW is calculated by the controller of the AFM tip using Hooke's law with the known spring constant (k) of $155\ \text{N/m}$ and the displacement (x) of the tip. The mechanical test of the Ag NW was recorded on video using a

CCD camera coupled to the microscope with recording speed of 15 frames per second (fps). The NW rested on the gold bondwire, and was finely approached towards the AFM tip at a 0.5 nm step by means of the piezotube. A detailed review about the strain/rate and displacement is reported by Greer et al [31] in which the plasticity study is analyzed after the elastic deformation in nanostructures and their mechanical properties changes as function of the size. From the video in supplementary information it was possible to analyze the mechanical response in the experiment of the Ag NW, in both regimens elastic and plastic, to an applied load. The strain distributed in the nanowire can be observed in the contrast changes during the experiment specifically after 55 seconds in the video recorded the strain changes are clearly observed a similar in situ experiment was performed by Chen et al [32-33]. The step considering the spring constant of the tip and the maximum displacement we measured a force around 3 kN. During the experiment the distribution of strain is observed and it has been simulated by finite element method available at supplementary information Figure S1 and the video. In order to obtain the Young modulus (E) of the Ag NWs during in situ three point bend testing we used the case of the uniformly distributed load, from the elastic theory of deflection.

The equations of the calculations are properly explained in the supplementary material as well as the properties of the geometry of the pentagonal nanowire such as the moment of inertia, area and centroid. The measured and calculated Young's modulus of the beam during the frames of the Figures 3(a) and 3(b) is 108 GPa. This number has been calculated in the first stage of the deformation, which the applied load begins to fracture and completely separates the nanowire into two strands. Figure 3 shows a series of frames of the point of contact to the tip to the moment of complete fracture, Figures 3(c) to 3(e) are part of the plastic deformation of the nano-beam until its fracture observed in figure (3f). During the deformation process it was possible to observe

contrast lines related to surface stresses moving rapidly along the NW, resembling a thin membrane on the surface of the NW. Higher density of contrast lines were observed close to the area where the load was applied. A careful observation of the area of the NW in close proximity with the AFM tip, revealed a region without contrast lines which can be associated to the compressive stress, and beneath that region, another with contrast lines associated to tensile stress of the NW. Moreover, while the Ag NW is being deflected, tensile stress is higher in the opposite side where the load is being applied, as revealed by the higher density of tensile contrast lines. However, failure of the pentagonal Ag NW started on the same side where the load was applied, and continue through the center of the NW.

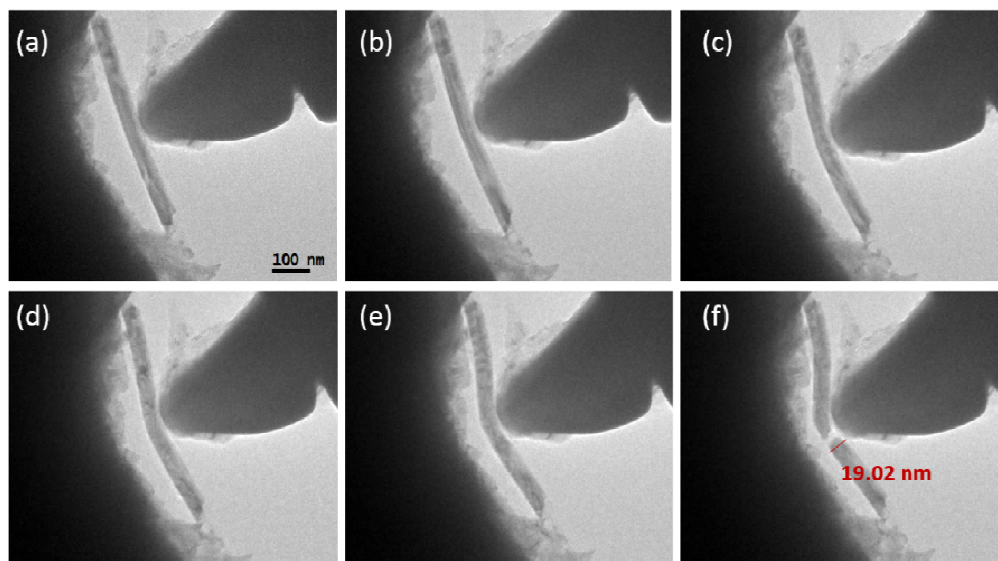


Figure 3 – Image sequence of the rupture of a silver nanowire using an AFM tip. A series of frames of the AFM tip making contact with the NW until total rupture of it due to high load pressure.

Finally, the NW diameter decreases, the Ag NW suffers plastic deformation at a maximum deflection of 65 nm and it fractures by necking. As shown in the video 1 in the supplementary

information, the instant the NW and the AFM tip get into contact, contrast lines appear on the NW surface, which are related to induced stresses onto the crystalline structure of the NW due to the applied load. Research on the matter of elastic properties of nanowires has concluded that the elasticity modulus of nano-scale materials should take into account the surface energy of nanostructures due to their large surface area. For instance He et al. [34] have shown explicit solutions about the dependence of the surface effect and the Young's modulus of nanowires considering two boundary conditions as follows: simply supported and fixed-fixed. He et al. conclude that there is a size dependence in silver NWs in their Young's moduli, when the diameter of the NWs decreases they behave like stiffer materials. Stiffer modulus for silver NWs when the nanowire is deformed in the (100) planes compared with the (111) planes [34]. In our experiment we have applied the load on the (100) planes and the experimental setup corresponds to the simply supported nanowire, the increase in the Young's modulus that we measured experimentally is in agreement with the modulus calculated by He et al. in the (001) planes. We have included a schematic representation of the crystalline orientation of the pentagonal silver nanowires in supplementary information as well as the crystalline orientation mapping obtained by precession electron diffraction-assisted automated crystal orientation mapping [35-36].

The fracture toughness of the Ag NW can also be calculated. Using the stress intensity factor of the material ($\sigma_F = F/\pi a$) the critical intensity fracture one can determine the resistance of the NW until rupture. The fracture is determined by a function of the fraction of the length of a crack over the diameter of the NW $K_{IC} = \sigma_F \sqrt{\pi c} f\left(\frac{c}{a}\right)$ where c is the length of fracture [37]. The stress intensity factor of the NW at a fracture length of 19 nm as shown in Figure 3(f) was calculated to be 186 N/m. Therefore, the fracture toughness could be calculated at a 38% of fracture to be $K_{IC} = 18.5 \text{ MN}/\text{nm}^{3/2}$.

AFM nanoindentation measurements are based on the force plots acquired (on seven nanowires) at five different points of the nanostructure; the tensile modulus in each plot was obtained using a customized MATLAB program with a modified Hertz model that correlate the data of the applied force ‘F’ and the indentation depth ‘ δ ’ of the tip $\delta_s^3 = \left(\frac{3}{4E_{TOT}}\right)^2 \frac{F^2}{R}$ [38]. Figure 4 shows the height profile of a silver nanowire and the elasticity distribution values obtained for the experimental indentations.

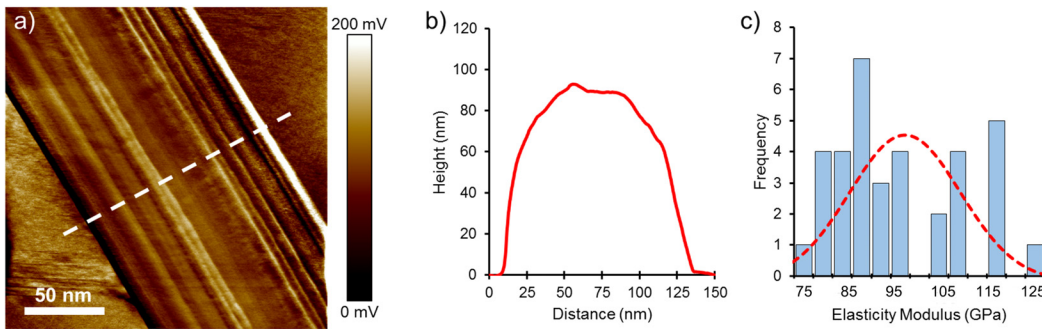


Figure 4 –a) Contact-Friction image of a silver nanowire used for the nanoindentation experiments. b) Height profile of the nanowire highlighted in a). c) Histogram of the effective elastic modulus computed for the approach force plots obtained in contact mode.

The Young's modulus attained from direct experiments using a silicon nitride tip was 97.2 ± 10.9 GPa. The bulk modulus for silver is around 81 GPa and reported results on AgNW is 94 GPa for this diameter scale [39]. One of the potential causes for this disagreement may be due to different experimental setup and methods. As the diameter of the nanowire becomes smaller, any imprecision of the dimensions of the specimen may have a significant effect on the obtained values. This includes the pentagonal cross-section geometry of the as synthesized samples and if the bending experiment was realized with the AgNW deposited on a flat surface or fixed only at its ends.

4. Conclusion

Our observations show the complete mechanical behavior from elastic deformation until fracture of a Silver NW in situ TEM. Because of the method in which the fracture is observed through the TEM, it provides a definite experimental results on the process of rupture as well as live feedback and visual confirmation of the fracture in real time. The experiment showed that the Ag NW in a three point bending test that had a Young's Modulus at 108 GPa. In comparison to the indentation performed using an AFM with the Ag NW on a flat surface without fracture that showed a 97.2 GPa in counterpart with its bulk modulus value of 81 GPa. We can conclude that we measured stiffer Young's modulus in Ag Nws until their fracture performed at individual nanowires.

Acknowledgments

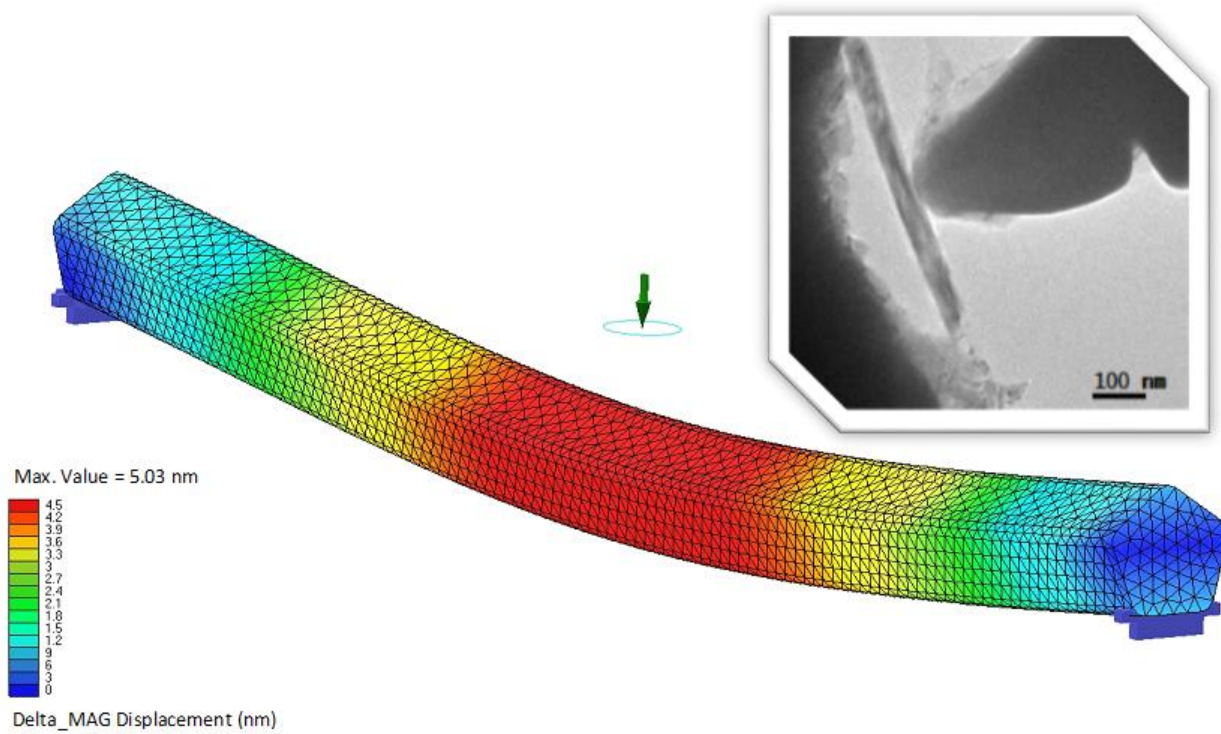
The authors would like to acknowledge the Welch Foundation (AX-1615) and the Department of Defense #64756-RT-REP. The microscopy work was supported by the National Institute on Minority Health and Health Disparities (NIMHD) in the program Research Centers in Minority Institutions Program (RCMI) Nanotechnology and Human Health Core (G12MD007591). The authors would also like to acknowledge the Mexican Council for Science and Technology, CONACYT # 250836 (Mexico) through the national scholarship and the International Center for Nanotechnology and Advanced Materials (ICNAM).

References

- [1] G. Casillas, J.P. Palomares-Baez, J.L. Rodriguez-Lopez, J. Luo, A. Ponce, R. Esparza, J.J. Velazquez-Salazar, A. Hurtado-Macias, J. Gonzalez-Hernandez, M. Jose-Yacaman, *Philos. Mag.* 92 (2012) 4437-4453.
- [2] D. Alducin, G. Casillas, F. Mendoza-Santoyo, A. Ponce, M. Jose-Yacaman, *J. Nanopart. Res.* 17:203 (2015) 1-7.
- [3] G. Casillas, U. Santiago, H. Barron, D. Alducin, A. Ponce, M. José-Yacaman, *J. Phys. Chem. C*, 119 (2015) 710–715.
- [4] J. Cantu-Valle, I. Betancourt, J.E. Sanchez, F. Ruiz-Zepeda, M.M. Maqableh, F. Mendoza-Santoyo, B.J.H. Stadler, A. Ponce, *J. Appl. Phys.* 118 (2015) 024302.
- [5] H. Diltbacher, A. Hohenau, D. Wagner, U. Kreibig, M. Rogers, F. Hofer, F. R. Aussenegg, J. R. Krenn, *Phys. Rev. Lett.* 95 (2005) 257403.
- [6] A. L. Pyayt, B. Wiley B, Y. Xia, A. Chen, L. Dalton, *Nature Nanotech.* 3 (2008) 660-665.
- [7] A. Tao, F. Kim, C. Hess, J. Goldberger, R. He, Y. Sun, Y. Xia, P. Yang, *Nano Lett.* 3 (2003) 1229-1233.
- [8] Y. Cui, I. Y. Phang, R. S. Hedge, Y. H. Lee, X. Y. Ling, *ACS Photonics* 1 (2014) 631-637.
- [9] Y. Fang, Z. Li, Y. Huang, S. Zhang, P. Nordlander, N. J. Halas, H. Xu, *Nano Lett.* 10 (2010) 1950-1964.
- [10] S. A. Maier, P. G. Kik, H. A. Atwater, S. Meltzer, E. Harel, B. E. Koel, A. A.G. Requicha, *Nature Mater.* 2(2003) 229-232.
- [11] S. Lal, S. Link, N. J. Halas, *Nature Photonics* 1 (2007) 641-648.

- [12] U. Yogeswaran, S. M. Chen, *Sensors* 8 (2008) 290-313.
- [13] M. Reches, E. Gazit, *Science* 300 (2003) 625-627.
- [14] B.H. Hong, S.C. Bae, C.W. Lee, S. Jeong, K. S. Kim, *Science* 294 (2001) 348-351.
- [15] Y. Sun, B. Gates, B. Mayers, Y. Xia, *Nano Lett.* 2 (2002) 165-168.
- [16] Y. Gao, P. Jian, D. F. Liu, H. J. Yuan, X. Q. Yan, Z. P. Zhou, J. X. Wang, L. Song, L. F. Liu, W. Y. Zhou, G. Wang, C. Y. Wang, S. S. Xie, *Chem. Phys. Lett.* 380 (2003) 146-149.
- [17] P. Pocharal, Z. L. Wang, D. Ugarte, W. A. De Heer, *Science* 283 (1999) 1513-1516.
- [18] S. Cuenot, C. Fretigny, S. Demoustier-Champagne, B. Nysten, *J. Appl. Phys.* 93 (2003) 5650.
- [19] S. Cuenot, C. Fretigny, S. Demoustier-Champagne, B. Nysten, *Phys. Rev.* 69 (2004) 165410.
- [20] D. A. Walters, L. M. Ericson, M. J. Casavant, J. Liu, D. T. Colbert, K. A. Smith, R. E. Smalley, *Appl. Phys. Lett.* 74 (1999) 3803-3805.
- [21] S. Cuenot, S. Demoustier-Champagne, B. Nysten, *Phys. Rev. Lett.* 85 (2000) 1690.
- [22] J. Song, X. Wang, E. Riedo, Z. L. Wang, *Nano Lett.* 5 (2005) 1954-1958.
- [23] A. S. Paulo, J. Bokor, R. T. Howe, R. He, P. Yang, D. Gao, C. Carraro, R. Maboudian, *Appl. Phys. Lett.* 87 (2005) 053111.
- [24] Y. Zhu, N. Moldovan, H. D. Espinosa, *Appl. Phys. Lett.* 86 (2005) 013506.
- [25] M. F. Yu, O. Lourie, M. J. Dyer, K. Moloni, T. F. Kelly, R. S. Ruoff, *Science* 287 (2000) 637-640.
- [26] Y. Chen, B. Dorgan, D. McIlroy, D. Aston, *J. Appl. Phys.* 100 (2006) 104301.

- [27] B. Wu, A. Heidelberg, J. J. Boland, J. E. Sader, X. Ming, Y. Dong, *Nano Lett.* 6(2006) 468-472.
- [28] B. Wiley, Y. Sun, Y. Xia, *Acc.Chem. Res.* 40 (2007) 1067–1076.
- [29] H. M. Ghassemi, C. H. Lee, Y. K. Yap, *J. Appl.Phys.*108 (2010) 024314.
- [30] D. Goldberg, X.D. Bai, M. Mitome, *Acta Mater.*55 (2007) 1293-1298.
- [31] J. R. Greer, J. T. M. De Hosson, *Prog. Mater Sci.*56 (2011) 654-724.
- [32] C. Q. Chen, Y. T. Pei, O. Kuzmin, Z. F. Zhang, E. Ma, J. T. M. De Hosson, *Phys. Rev. B* 83 (2011) 180201(R).
- [33] C. Q. Chen, Y. T. Pei, J. T. M. De Hosson, *Acta Mater.*58 (2010) 189-200.
- [34] J. He, C. M. Lilley, *Nano Lett.* 8 (2008) 1798-1802.
- [35] E. F. Rauch, M. Véron, *Mater. Charact.* 98 (2014) 1-9.
- [36] F. Ruiz-Zepeda, Y.L. Casallas-Moreno, J. Cantu-Valle, D. Alducin, U. Santiago, M. Jose-Yacaman, M. Lopez-Lopez and A. Ponce, *Microsc. Res. Tech.* 77 (2014) 980-985.
- [37] X. Zhu, J. A. Joyce, *Eng. Fract. Mech.* 85 (2012) 1-46.
- [38] H. Butt, B. Cappella, M. Kappa, *Surf. Sci. Rep.* 59 (2005) 1-152.
- [39] Y. Zhu, Q. Qingquan, F. Xu, *Phys Rev B* 85 (2012) 045443.



Mechanical deformation of an individual silver nanowire within a transmission electron microscope